



Hybridization of carbon-dots with ZnO nanoparticles of different sizes

Mulugeta Tesema Efa^a, Toyoko Imae^{a,b,*}

^a Graduate Institute of Applied Science and Technology, National Taiwan University of Science and Technology, Taipei 10607, Taiwan

^b Department of Chemical Engineering, National Taiwan University of Science and Technology, Taipei 10607, Taiwan



ARTICLE INFO

Article history:

Received 25 November 2017

Revised 5 February 2018

Accepted 6 February 2018

Available online 7 March 2018

Keywords:

Carbon dot
Zinc oxide nanoparticle
Hybrid
Specific surface area
Band gap

ABSTRACT

ZnO nanoparticles were hybridized with carbon dots (Cdots) and the hybrids were characterized. ZnO(100) and ZnO(20) with particle sizes of 94 and 20 nm, respectively, were synthesized by calcination and polyol solvent methods, respectively. The morphology, size and crystallinity of ZnO nanoparticles were not varied by the addition of Cdots. The spectroscopic results indicated the successful attachment of Cdots to ZnO nanoparticles. The specific surface area of ZnO(20) was larger than ZnO(100) and increased with the hybridization of Cdots. When the amount of ethylenediamine against citric acid between raw materials of Cdots was increased, the existence of nitrogen in Cdots became recognized. The band gap increased with decreasing particle size, and the addition of Cdots decreased the band gap of ZnO. Thus, these results suggest that the hybrids of ZnO with Cdots may exert the performance on photocatalysis and photovoltaic electrochemistry.

© 2018 Taiwan Institute of Chemical Engineers. Published by Elsevier B.V. All rights reserved.

1. Introduction

Carbon dots (Cdots), which are one of the latest nano-allotropes of carbon materials, take a size of few nm and possess a property of quantum dots. After the pioneering synthesis of Cdots from carbon nanotube, various procedures of the Cdots production from different raw materials have been reported, and their characterizations have been performed [1,2]. Especially, due to their easy synthesis, biocompatibility, excellent stability and water dispersibility, Cdots attract researchers who focus on the applications [3–10]. Incidentally, metal oxides are highly valuing in photovoltaic research as excellent semiconducting materials, which possess an adequate band gap energy and absorbed energy of sun light [11]. For instance, metal oxides such as titanium dioxide (TiO₂), zinc oxide (ZnO) and tin dioxide (SnO₂) are applicable to photocatalysts and dye-sensitized solar cells [12–17]. Cdots are expected to be easily incorporated in such metal oxides and to effectively increase light absorption of metal oxide-Cdots composites in the visible region, leading to massive photocurrents. The metal oxide-Cdots composites also may present an energetically favorable conduction band and an electrochemical activity.

In the present work, the characterization of ZnO influenced by addition of Cdots has been investigated on ZnO nanoparticles with different particle sizes, which exhibited significantly different ef-

fects. The effects of Cdots were examined at the different amounts of nitrogen content in Cdots, which were varied by changing the ratio of raw materials (citric acid and ethylenediamine). Thus, the Cdots will be expected to be the promising additive for enhancing semiconductive performance of ZnO.

2. Experimental section

Zinc nitrate hexahydrate (98%), oxalic acid dihydrate (99.5%), ethylene glycol (99+%), ethylenediamine (99%), isopropanol (99.5%) and citric acid anhydrous (99%) were purchased from Acros organics (USA). Sodium hydroxide pellet (95%) was obtained from J.T. Baker (Sweden).

ZnO nanoparticles were prepared using two methods. On the calcination synthesis, an aqueous solution (100 ml) of zinc nitrate hexahydrate (0.4 M, 5.94 g) was heated at 80 °C and was added quickly to an aqueous solution (100 ml) of oxalic acid (0.6 M, 3.78 g) at 80 °C [14,15]. Then the resulting dispersion was sonicated for 20 min, stirred for 4 h, filtered, washed several times with water and air-dried for 12 h. After zinc oxalate was calcined for 12 h at 450 °C, the product was allowed to cool down to room temperature. On the polyol solvent synthesis method, zinc nitrate hexahydrate (7.45 g) and NaOH (1 g) dissolved separately in ethylene glycol (25 ml) were mixed at pH 11.5 and stirred for 1 h at 80 °C. Precipitates were washed by centrifugation using acetone, ethanol and water and air-dried overnight.

Cdots with different nitrogen contents were synthesized via a method like that described previously [3,9,10] but with minor

* Corresponding author at: Department of Chemical Engineering, National Taiwan University of Science and Technology, Taipei 10607, Taiwan.

E-mail address: imae@mail.ntust.edu.tw (T. Imae).

modifications. Citric acid anhydrous (1 g) was dissolved in water (70 ml) and ethylenediamine (0.30 and 0.6 ml) was added to be the number ratios of NH_2 group in ethylenediamine against COOH group in citric acid of 1:1 and 2:1, respectively, which were hereafter described Cdots($x=1$ and 2). After the mixture was stirred for 30 min at room temperature, it was hydrothermally carbonized in an autoclave for 5 h at 250 °C and stood to cool. The solvent was evaporated and the resulted Cdots were dried for 3 h at 100 °C. ZnO (400 mg) in isopropanol (2 ml) and Cdots (48 mg, 10% wt) in water (2 ml) were mixed, sonicated for 10 min and stirred for 4 h at room temperature. ZnO@Cdots were filtered, washed several times with water, air-dried overnight and heat-dried at 100 °C for 3 h.

The transmission electron microscopic (TEM) images were acquired using a JEOL JEM-2100 operating at an acceleration voltage of 120 kV. The carbon-coated copper grid was drop-coated by an isopropanol dispersion of ZnO@Cdots and the solvent was evaporated in air. The X-ray diffraction (XRD) patterns were recorded at 20–80° on a Rigaku D/Max-kA diffractometer using $\text{CuK}\alpha$ radiation (1.54 Å) at 40 kV and 30 mA. Sample powders were dried at 100 °C for 3 h before measurement. X-ray photoelectron spectroscopic (XPS) measurement was performed on a Thermo Scientific K-alpha instrument. Fourier transform infrared (FTIR) absorption spectra were recorded using a NICOLET700 instrument at an accumulative scan of 64 times. An isopropanol solution of ZnO@Cdots was dropped on CaF_2 pellet and dried. The ultraviolet (UV)–visible absorption spectra were recorded using a Jasco V-670 series spectrometer. The quartz plate was dipped into the concentrated dispersion of sample powder in isopropanol, dried in air and supplied for measurement. The nitrogen adsorption experiment was done at 77 K using a Brunauer–Emmett–Teller (BET) surface area analyzer (BELSORB Max) after pre-heat treatment of 200 mg sample solid at 300 °C for 3 h.

3. Results and discussion

While ZnO was prepared by two different synthesis methods of calcination and polyol solvent methods [14,15], Cdots were synthesized by the hydrothermal method from citric acid and ethylenediamine [3,9,10] and hybridized with ZnO by the mixing procedure. Fig. 1A exhibits TEM images of two ZnO particles and their hybrids with Cdots (ZnO@Cdots(1)). Both ZnO particles took polyhedral shape but their sizes were different about 5 times. Moreover, their size and shape were not remarkably changed after hybridization with Cdots. Fig. 1B shows the size distributions obtained by sampling particles in TEM images. The particle average sizes were 93.9 ± 23.9 and 20.4 ± 9.6 nm for ZnO synthesized by calcination and polyol solvent methods, respectively. Thus, hereafter, the former and latter ZnO particles are called ZnO(100) and Zn(20), respectively. Incidentally, the average sizes (94.4 ± 24.4 and 20.5 ± 9.5 nm, respectively) of ZnO(100)@Cdots(1) and ZnO(20)@Cdots(1) were consistent with those of the corresponding ZnO.

Fig. 2 shows XRD patterns of ZnO and ZnO@Cdots with different ZnO sizes and NH_2 contents in Cdots. Both XRD patterns of ZnO(100) and ZnO(20) correspond to the hexagonal wurtzite structure (JPCDS No 36–1451). The values of lattice parameter were $a=3.22$ Å, $c=5.21$ Å and c/a ratio = 1.628 for ZnO(100) and $a=3.24$ Å, $c=5.28$ Å and $c/a=1.629$ for ZnO(20), which were close to the standard $c/a=1.633$ for wurtzite structure [16]. The XRD patterns of ZnO@Cdots, regardless of amine content, were well consistent with those of corresponding ZnO and the appearance of new peaks assigned to Cdots were not clearly confirmed in the XRD patterns of ZnO@Cdots owing to the amorphous structure of Cdots [6,9]. That is, the crystallinity of ZnO nanoparticles, as well as their morphology and size, was not influenced by the addition

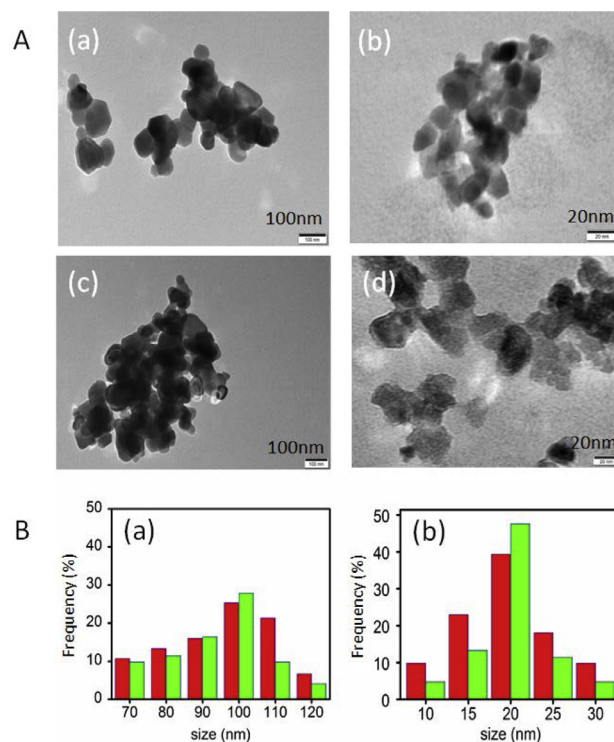


Fig. 1. (A) TEM images of (a) ZnO(100), (b) ZnO(20), (c) Zn(100)@Cdots(1) and (d) Zn(20)@Cdots(1). (B) Particle size distribution of (a) (red) Zn(100) and (green) Zn(100)@Cdots(1) and (b) (red) Zn(20) and (green) Zn(20)@Cdots(1). (For interpretation of the references to color in this figure legend, the reader is referred to the web version of this article.)

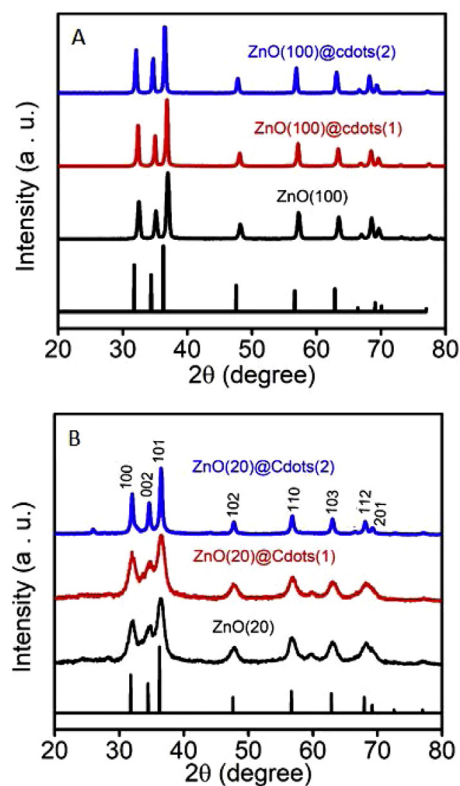


Fig. 2. X-ray diffraction patterns of (A) ZnO(100), ZnO(100)@Cdots(1) and ZnO(100)@Cdots(2) and (B) ZnO(20), ZnO(20)@Cdots(1) and ZnO(20)@Cdots(2). Inset the expected peak positions from a crystallographic database.

Table 1
IR absorption bands (at cm^{-1}) and their assignments of Cdots, ZnO and ZnO@Cdots(1). (w: weak band, sh: shoulder band).

Assignment	Cdots(1)	ZnO(100)	ZnO(100)@Cdots(1)	ZnO(20)	ZnO(20)@Cdots(1)
O–H stretching	3500		3500	3500	3500
	3300sh		3350	3300sh	3300
C–H stretching	2960 w				
C=O and COO ⁻ stretching, NH ₂ bending	1660		1700sh	(1650 w)	1670
	1550		1580 w		1560
		(1500 w)	(1500 w)		
O–H bending	1390 w	(1350 w)	1400 w	1400	1400

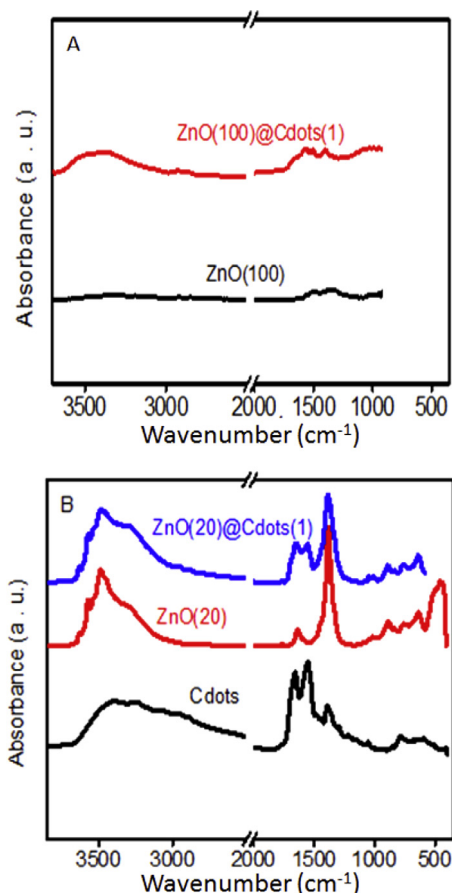


Fig. 3. FTIR absorption spectra of (A) ZnO(100) and ZnO(100)@Cdots(1) and (B) ZnO(20), ZnO(20)@Cdots(1) and Cdots(1).

of Cdots. The broadening of XRD peaks seen in cases of ZnO(20) and ZnO(20)@Cdots(1) in Fig. 2B suggests that their nanoparticles are small in size, although the sharpness seems to be increasing on ZnO(20)@Cdots(2) [15].

FTIR absorption bands of ZnO@Cdots(1) are compared to those of ZnO and Cdots in Fig. 3 and Table 1. While ZnO(100) did not display any characteristic IR bands except weak bands around 1500 and 1350 cm^{-1} , new bands on ZnO(100)@Cdots(1) appeared at 3500, 3350, 1700 and 1580 cm^{-1} , which were attributed to IR bands of Cdots [6,9,10]. Meanwhile, main IR bands of ZnO(20) observed at 3500 and 1400 cm^{-1} can be assigned to O–H vibration modes of ethylene glycol, which was used on the synthesis of ZnO(20) nanoparticles and adsorbed on the nanoparticle surface as stabilizer/protector. The additional IR bands on ZnO(20)@Cdots(1) appeared at 1670 and 1560 cm^{-1} can be attributed to the vibration modes originated in Cdots. Then, it can be confirmed that characteristic IR bands of both ZnO(20) and Cdots(1) were observed on

ZnO(20)@Cdots(1). Thus, the FTIR results support that Cdots have been successfully attached to ZnO nanoparticles.

The full XPS survey scan of ZnO(20)@Cdots and ZnO (Fig. 4A) exhibited the distinctive peaks that are assigned to C1s, N1s, O1s and Zn2p. The chemical composition and species in the particles can be characterized by fine analysis in XPS. The fine peaks of each element are shown in Fig. 4B, which includes deconvoluted line spectra. The binding energy values and area intensities of deconvoluted species are listed in Table 2 in comparison with those of Cdots. The Zn2p^{3/2} and Zn2p^{1/2} species appeared at binding energies of 1023 and 1046 eV, respectively, for ZnO(20)@Cdots(1), ZnO(20)@Cdots(2) and ZnO [16] and these binding energies did not change before and after hybridization with Cdots.

On a C1s peak, ZnO possessed two deconvoluted species, which are attributed to alkyl (sp^3) C–C and C–OH of ethylene glycol adsorbed on ZnO on the process of the synthesis, as clarified from IR absorption spectra. On the other hand, among three main deconvoluted species of Cdots, a species of lowest binding energy is assigned to C=C and C–C bonds of aromatic (sp^2) carbons and two peaks of higher binding energies is due to the contribution of C–COOH, C–NH₂ and alkyl C–C carbons [6]. Thus, four species of ZnO(20)@Cdots(1) can be said to be contributed by both ZnO and Cdots. Similar contribution was confirmed even from O1s peak: While the O1s peak of ZnO was deconvoluted into two species of ZnO main unit and C–OH from ethylene glycol and the O1s peak of Cdots was contributed from C=O and C–OH of COOH, ZnO(20)@Cdots(1) exhibited four deconvoluted species contributed from ZnO and Cdots.

Although all characteristic species appeared for ZnO(20)@Cdots(1) could be observed even for ZnO(20)@Cdots(2) as well, XPS analysis indicated the additional species originating from much amount of nitrogen (NH₂) incorporation in ZnO(20)@Cdots(2), although they were not recognized in ZnO(20)@Cdots(1) because of less amount of nitrogen existence. The deconvolution of C1s and N1s peaks indicated additional species of C–NH₂ at 286.6, 400.1 and 402.3 eV. Incidentally, Cdots appeared an N1s peak of C–NH₂ at 399.9 eV but did not distinguish C1s peak of C–NH₂ [6,18,19].

The nitrogen adsorption/desorption isotherms at 77 K were measured for ZnO(100), ZnO(20) and ZnO(20)@Cdots(2) powders. The isotherms are plotted in Fig. 5 and the determined BET parameters are listed in Table 3. The specific surface area increased about 5 times from ZnO(100) to ZnO(20) and 8% by adding Cdots on ZnO(20). Pore volume also increased with decreasing ZnO size, but it decreased with addition of Cdots, indicating the stop-up of the pores by Cdots.

The band gap of ZnO and ZnO@Cdots nanoparticles can be calculated by means of Tauc's plot given by an equation of $(\alpha h\nu)^2 = B(h\nu - E_g)$, where α is the absorption coefficient, $h\nu$ is the photon energy, B is the constant and E_g is the band gap energy [16,20,21]. Then on the curve of $(\alpha h\nu)^2$ as a function of $h\nu$ as shown in Fig. 6, which was recalculated from UV–visible absorption spectra, the $h\nu$ value at the extrapolation of linear line to

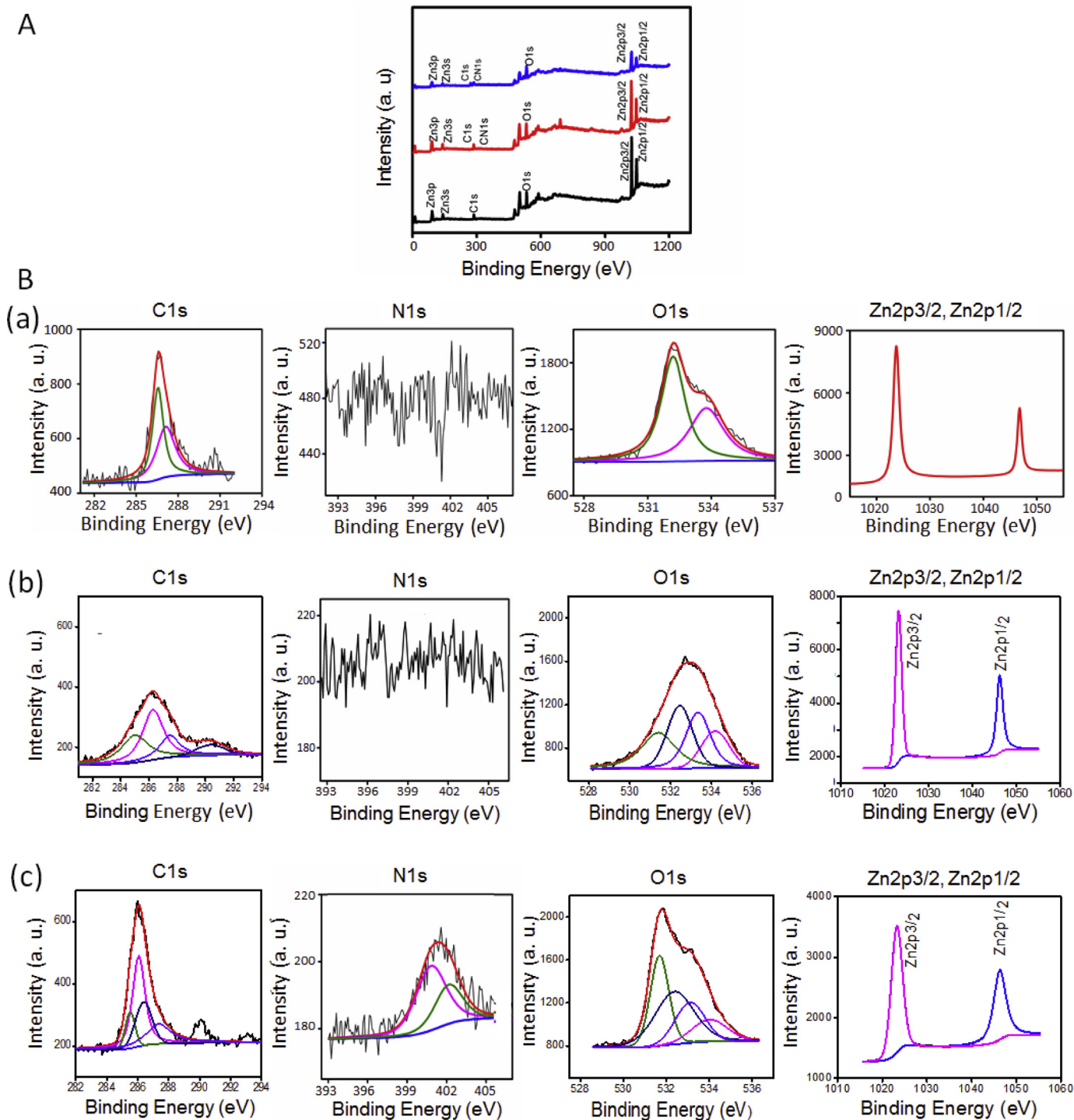


Fig. 4. (A) XPS full survey spectra of (black) ZnO(20), (blue) ZnO(20)@Cdots(1) and (red) ZnO(20)@Cdots(2). (B) XPS fine spectra of C1s, N1s, O1s, Zn2p3/2 and Zn2p1/2 of (a) ZnO(20), (b) ZnO(20)@Cdots(1) and (c) ZnO(20)@Cdots(2). (For interpretation of the references to color in this figure legend, the reader is referred to the web version of this article.)

$(\alpha h\nu)^2 = 0$ is the band gap value. Thus, the band gap energies were evaluated and listed in Table 4.

It can be noted that the optical band gap depended on the particle size: A blue shift of UV–visible absorption band of ZnO occurred, i.e. the band gap increased with decreasing particle size from 94 nm to 20 nm. Incidentally, ZnO aggregates displayed lower band gap of 3.02 eV [16]. The band gap between valence band and conduction band generally occurs inside the nanoparti-

cle. When the particle size decreases, the electron is confined in the particle (confinement effect), leading to the increase in band gap energy and the quantization of band levels. Thus, the energy level spacing increases with decreasing the size dimension. On the other hand, the addition of Cdots decreased the band gap of ZnO. Similar phenomenon was reported even by adding ZrS₂ to ZnO [16]. This is due to the decrease of conduction band level by additives.

Table 2
Binding energy (BE) and area intensity obtained from XPS of ZnO(20), ZnO(20)@Cdots and Cdots(1).

Element	ZnO(20)		ZnO(20)@Cdots(1)		ZnO(20)@Cdots(2)		Cdots(1)		Assignment
	BE (eV)	Area intensity	BE (eV)	Area intensity	BE (eV)	Area intensity	BE (eV)	Area intensity	
C1s			284.9	240.0	285.5	309.0	284.6	208.1	CC (aromatic)
			286.2	323.1	286.0	491.7	285.6	42.8	C-OOH
					286.6	372.5			C-NH ₂
			287.2	642.3	287.6	341.6	287.9	55.4	C-C (alkyl)
			288.6	787.2	290.4	268.2	(288.6)	(4.7)	C-OH
N1s			298.2	209.2	400.1	198.5	399.9	55.4	C-NH ₂
					402.3	185.7			
O1s			531.3	946.8	531.4	1646.3	(531.1)	(21.8)	C=O (COOH)
			532.4	1196.7	532.1	1313.6	532.2	138.9	C-OH(EGC)
			533.3	1334.5	533.1	1205.1			C-OH(COOH)
			534.5	959.8	534.2	1047.2	533.1	115.7	O ²⁻ (ZnO)
			533.8	1362.6					Zn ⁺² (ZnO)
Zn2p3/2	1023.7	12,279.5	1023.2	7453.0	1023.2	3529.5			

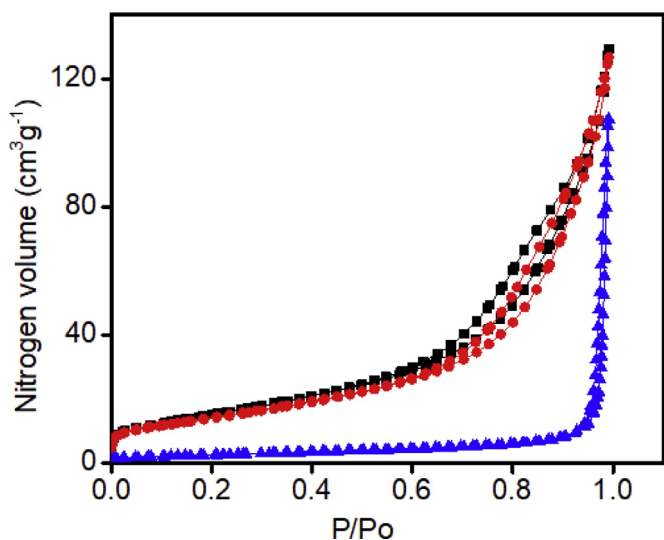


Fig. 5. Nitrogen adsorption–desorption isotherm at 77 K. (blue) ZnO(100), (red) ZnO(20) and (black) ZnO(20)@Cdots(2). (For interpretation of the references to color in this figure legend, the reader is referred to the web version of this article.)

Table 3
BET analysis of adsorption isotherm of ZnO(100), ZnO(20) and ZnO(20)@Cdots(2).

Nanoparticle	Specific surface area (m ² /g)	Pore volume (cm ³ /g)
ZnO(100)	9.09	0.153
ZnO(20)	51.5	0.195
ZnO(20)@Cdots(2)	55.7	0.191

Table 4
Band gap of ZnO and ZnO@Cdots.

Nanoparticle	Band gap (eV)	Nanoparticle	Band gap (eV)
ZnO(100)	3.25	ZnO(20)	3.35
ZnO(100)@Cdots(1)	3.20	ZnO(20)@Cdots(1)	3.32
ZnO(100)@Cdots(2)	3.18	ZnO(20)@Cdots(2)	3.10

4. Conclusions

In this work, composite nanoparticles consisting of two sizes of ZnO by the addition of Cdots were synthesized and characterized. While the calcination method produced large ZnO nanoparticles, the nanoparticles from the polyol solvent method were small. Cdots were synthesized from citric acid and ethylenediamine by the hydrothermal method and, thus, the content of nitrogen in Cdots can be easily varied by changing the blended amount of citric acid and ethylenediamine. Cdots are readily adsorbed on ZnO

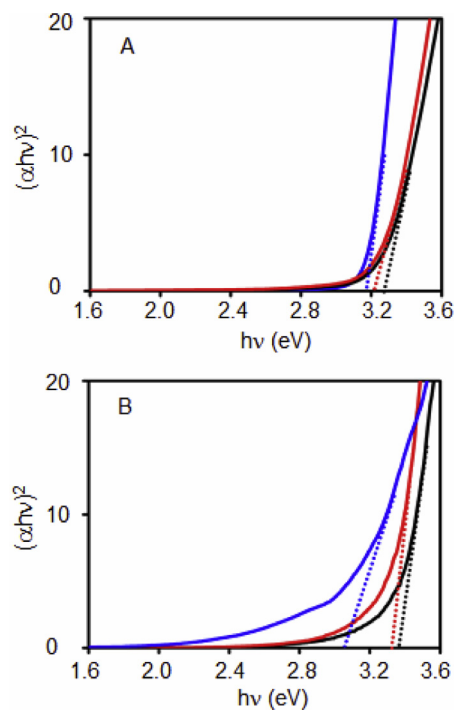


Fig. 6. Tauc's plots for band gap determination of ZnO and ZnO@Cdots. (A) (black) ZnO(100), (red) ZnO(100)@Cdots(1) and (blue) ZnO(100)@Cdots(2). (B) (black) ZnO(20), (red) ZnO(20)@Cdots(1) and (blue) ZnO(20)@Cdots(2). (For interpretation of the references to color in this figure legend, the reader is referred to the web version of this article.)

by simple mixing. The hybridization of Cdots on ZnO can be confirmed by spectroscopic techniques. Although the addition of Cdots did not influence on the morphology, size and crystallography of ZnO, it contributed to the variation of specific surface area and band gap of ZnO. ZnO of small size possesses large surface area per volume and thus it may present higher performance on catalysis than ZnO of large size. Small particle size is favorable for quick attainment of photoexcited electron–hole pair separation in conducting ZnO nanoparticles. Moreover, the adsorption of Cdots on ZnO may enhance such effects. Thus, these characteristics of composite nanoparticles are expected to effect the photocatalytic and photovoltaic performances.

Acknowledgment

MTE gratefully acknowledges the financial support from National Taiwan University of Science and Technology, Taiwan, by a

student scholarship. We thank Dr. M.M.M. Ahmed for the measurements of XRD and BET and Mr. Kuku Wicaksono for the measurement of XPS of Cdots.

References

- [1] Xu X, Ray R, Gu Y, Ploehn HJ, Gearheart L, Raker K, et al. Electrophoretic analysis and purification of fluorescent single-walled carbon nanotube fragments. *J Am Chem Soc* 2004;126(40):12736–7.
- [2] Sun Y-P, Zhou B, Lin Y, Wang W, Fernando KAS, Pathak P, et al. Quantum-sized carbon dots for bright and colorful photoluminescence. *J Am Chem Soc* 2006;128(24):7756–7.
- [3] Krysmann MJ, Kelarakis A, Dallas P, Giannelis EP. Formation mechanism of carbonogenic nanoparticles with dual photoluminescence emission. *J Am Chem Soc* 2011;134(2):747–50.
- [4] Li Y, Hu Y, Zhao Y, Shi G, Deng L, Hou Y, et al. An electrochemical avenue to green-luminescent graphene quantum dots as potential electron-acceptors for photovoltaics. *Adv Mater* 2011;23(6):776–80.
- [5] Hsu P-C, Shih Z-Y, Lee C-H, Chang H-T. Synthesis and analytical applications of photoluminescent carbon nanodots. *Green Chem* 2012;14(4):917–20.
- [6] Prasanna A, Imae T. One-pot synthesis of fluorescent carbon dots from orange waste peels. *Ind Eng Chem Res* 2013;52(44):15673–8.
- [7] Wang Y, Hu A. Carbon quantum dots: synthesis, properties and applications. *J Mater Chem C* 2014;2(34):6921–39.
- [8] Wang J, Zhang P, Huang C, Liu G, Leung KC, Wang YX. High performance photoluminescent carbon dots for in vitro and in vivo bioimaging: effect of nitrogen doping ratios. *Langmuir* 2015;31(29):8063–73.
- [9] Hsu Y-H, Hsieh H-L, Viswanathan G, Voon SH, Kue CS, Saw WS, et al. Multifunctional carbon-coated magnetic sensing graphene oxide-cyclodextrin nanohybrid for potential cancer theranosis. *J Nanopart Res* 2017;19(11):359.
- [10] Devadas B, Imae T. An effect of carbon dots on conducting polymers for energy storage application. *ACS Sustainable Chem Eng* 2018(6):127–34.
- [11] Nakata K, Fujishima A. TiO₂ photocatalysis: design and applications. *J Photochem Photobiol C* 2012;13(3):169–89.
- [12] O'Regan B, Graetzel M. A low-cost, high-efficiency solar cell based on dye-sensitized colloidal titanium dioxide films. *Nature* 1991;353(6346):737–40.
- [13] Mrowetz M, Balcerski W, Colussi AJ, Hoffmann MR. Oxidative power of nitrogen-doped TiO₂ photocatalysts under visible illumination. *J Phys Chem B* 2004;108(45):17269–73.
- [14] Dutta V. Spray deposited ZnO nanostructured layers for dye sensitized solar cells. *Energy Proc* 2011(3):58–62.
- [15] Kumar V, Singh N, Kumar V, Purohit LP, Kapoor A, Ntwaeaborwa OM, et al. Doped zinc oxide window layers for dye sensitized solar cells. *J Appl Phys* 2013;114(13):134506. <http://dx.doi.org/10.1063/1.4824363>.
- [16] Krishnakumar B, Imae T, Miras J, Esquena J. Synthesis and azo dye photodegradation activity of ZrS₂-ZnO nano-composites. *Sep Purif Technol* 2014(132):281–8.
- [17] Krishnakumar B, Imae T. Chemically modified novel PAMAM-ZnO nanocomposite: synthesis, characterization and photocatalytic activity. *Appl Catal A: Gen* 2014(486):170–5.
- [18] Adhikari PD, Imae T, Motojima S. Selective immobilization of carbon micro coils on patterned substrates and their electrochemical behavior on ITO substrate. *J Chem Eng Chem* 2011;174(2-3):693–8.
- [19] György E, Pérez del Pino A, Logofatu C, Duta A, Isac L. Effect of nitrogen doping on wetting and photoactive properties of laser processed zinc oxide-graphene oxide nanocomposite layers. *J Appl Phys* 2014;116(2):024906–7.
- [20] Segets D, Matthew Lucas J, Klupp N. Determination of the quantum DotBand gap dependence on particle size from optical absorbance and transmission electron microscopy measurements. *ACS Nano* 2012;6(10):9021–32.
- [21] Rauwel P, Salumaa M, Aasna A, Galeckas A, Rauwel E. A review of the synthesis and photoluminescence properties of hybrid ZnO and carbon nanomaterials. *J Nanomater* 2016(2016). doi:10.1155/2016/5320625-37.